Distance and age of the massive stellar cluster Westerlund 1.
I. Parallax method using Gaia-EDR3

Felipe Navarete[1,2]★ ⓘ, Augusto Damineli[2] ⓘ, Aura E. Ramirez[2] ⓘ, Danilo F. Rocha[3,4] ⓘ,
Leonardo A. Almeida[4,5] ⓘ

[1]*SOAR Telescope/NSF's NOIRLab, Avda Juan Cisternas 1500, 1700000, La Serena, Chile*
[2]*Universidade de São Paulo, Instituto de Astronomia, Geofísica e Ciências Atmosféricas, Rua do Matão, 1226, São Paulo - SP, 05508-090, Brazil*
[3]*Observatório Nacional, R. Gen. José Cristino, 77 - Vasco da Gama, Rio de Janeiro - RJ, 20921-400, Brazil*
[4]*Programa de Pós-Graduação em Física, Universidade do Estado do Rio Grande do Norte, Mossoró - RN, 59610-210, Brazil*
[5]*Escola de Ciências e Tecnologia, Universidade Federal do Rio Grande do Norte, Natal - RN, 59072-970, Brazil*

ABSTRACT

Westerlund 1 (Wd 1) is one of the most massive young star clusters in the Milky Way. Although relevant for star formation and evolution, its fundamental parameters are not yet very well constrained. We aim to derive an accurate distance and provide constraints on the cluster age. We used the photometric and astrometric information available in the Gaia Early Data Release 3 (Gaia-EDR3) to infer its distance of $4.06^{+0.36}_{-0.34}$ kpc. Modelling of the eclipsing binary system W36, reported in Paper II, led to the distance of 4.03 ± 0.25 kpc, in agreement with the Gaia-EDR3 distance and, therefore, validating the parallax zero-point correction approach appropriate for red objects. The weighted average distance based on these two methods results in $d_{wd1} = 4.05 \pm 0.20$ kpc ($m - M = 13.04^{+0.11}_{-0.12}$ mag), which has an unprecedented accuracy of 5%. Using the Binary Population and Spectral Synthesis (BPASS) models for the Red Supergiants with solar abundance, we derived an age of 10.7 ± 1 Myr, in excellent agreement with recent work by Beasor & Davies ($10.4^{+1.3}_{-1.2}$ Myr) based on MIST evolutionary models. In Paper II, the age of W36B was reported to be 6.4 ± 0.5 Myr, supporting recent claims of a temporal spread of several Myrs for the star-forming process within Wd 1 instead of a single monolithic starburst episode scenario.

Key words: Astrometry and Celestial Mechanics: parallaxes – stars: distances – stars: supergiants – stars: Wolf–Rayet – Galaxy: open clusters and associations: individual: Westerlund 1

1 INTRODUCTION

The formation and evolution of massive stars is poorly known because massive stellar clusters are extremely rare within distances that their stellar population can be resolved. In this context, Westerlund 1 (henceforth Wd 1) is relevant, since it is potentially the most massive ($\sim 6 \times 10^4$ M$_\odot$, Portegies Zwart et al. 2010 and references therein) young stellar cluster (4-11 Myr, Beasor et al. 2021; Brandner et al. 2008; Gennaro et al. 2011) in our Galaxy. It is a local sibling of 30 Dor, although a little denser and less massive than this one. Wd 1 is located at ~ 10 times closer distance (3-5 kpc - Andersen et al. 2017; Kothes & Dougherty 2007; Davies & Beasor 2019; Beasor et al. 2021), making it an ideal template for investigating the massive stellar formation and evolution process in the nearby Universe, but still at a considerable large distance and extinction ($A_V \sim 11.5$, Damineli et al. 2016; Hosek et al. 2018) that precluded its fully characterisation until now. This massive cluster

harbours a large population of confirmed massive stars evolved off the Main Sequence (MS): four Red Supergiants (RSG), 24 Wolf-Rayets (WR), more than 100 Blue Giant and Supergiants OB stars, one magnetar, one Luminous Blue Variable (LBV), one B[e], and six Yellow Hypergiants (YHG) - a short-lived phase (Clark et al. 2005; Crowther et al. 2006; Muno et al. 2006; Negueruela et al. 2010). Given its large population of massive stars, Wd 1 is expected to generate more than a thousand supernovae explosions, producing a significant number of X- and γ-rays binaries, and the coalescence of some of them will likely generate gravitational waves (Abbott et al. 2020). Indeed, several X-ray binaries were already identified due to thermal X-rays produced by wind-wind collision in massive binaries (Skinner et al. 2006). The fraction of binaries is still not precisely known but is estimated to be a relatively large fraction of the Wd 1 stellar population ($> 70\%$, Crowther et al. 2006, Clark et al. 2019; $> 40\%$, Ritchie et al. 2021 - submitted)). Binarity among massive stars is relevant since $> 70\%$ of them will exchange mass with the companion, frequently leading to a binary merger (Sana et al. 2012) with potential for producing gravitational waves.

★ E-mail: felipe.navarete@noirlab.edu (FN)

The question of whether Wd 1 serves as a "golden-standard" laboratory for massive stellar evolution (Clark et al. 2014) is still under debate. There is a large age discrepancy between different methods for Wd 1. The pre-MS sequence population indicates an age of ~ 5-7 Myr (Andersen et al. 2017), much younger than that of the less-luminous RSG (~ 11 Myr, Beasor et al. 2021, leaving the door open for more than a unique episode of star formation over time. Since extinction and distance are not well constrained for Wd 1, absolute luminosities are uncertain, impacting the determination of individual stellar ages and, thus, the age of the cluster itself.

The presence of RSGs and WRs in a coeval cluster would indicate a narrow range of possible ages in a scenario of stars evolving in isolation (~ 5 Myr, Clark et al. 2005). However, binary interactions shape the unique cohort of hypergiant stars, with mass-stripped primaries, rejuvenated secondaries, and merger products (Clark et al. 2020). Beasor et al. (2021) proposed that stars in Wd 1 formed over a period of several Myr, similar to R136/NGC 2070, based on the evolved population (Schneider et al. 2018). However, this cluster shows many sub-clusters distributed throughout its confines which does not seem to be the case for Wd 1. The same authors point to the difference between the HRD of Wd 1 and RSGC1 (Davies et al. 2008). Although RSGC1 has a total mass and the age of RSGs similar to those in Wd 1, it does not show any WR and is prone to represent a single starburst.

The reddening law and extinction were accurately determined by Damineli et al. (2016, hereafter D16) using colour indices of bright cluster members calibrated from spectral types reported by Clark et al. (2005); Ritchie et al. (2009); Negueruela et al. (2010); Clark et al. (2020) and JHK_s photometry measurements combining telescopes of different diameters (4-m, 60-cm and mask aperture of 2-cm). Hosek et al. (2018) used JHK_s photometry and modelled the colour excesses of MS members by adopting a 5 Myr isochrone. They found good agreement between the average extinction to the cluster ($A_{Ks} = 0.78 \pm 0.16$ mag) with that reported by D16 ($A_{Ks} = 0.74 \pm 0.01$ mag). Hosek et al. (2018) also derived a steep optical/NIR reddening law similar to the of D16 and showed that it is not compatible with previous ones, even with those tuned to the inner Galaxy (Galactic Bulge, outside of the Galactic Plane), such as reported by Nishiyama et al. (2009). To date, the reddening law and the mean A_{Ks} extinction are the best well-constrained parameters for the Wd 1 cluster.

Previous distance determinations, however, have not converged to a ~ 10% accuracy, which is an uncertainty level desired for this case. The first suggestion for the Wd 1 distance was made by Westerlund (1961) by assuming it was located on the Sagittarius arm, at d > 1.4 kpc. Kothes & Dougherty (2007) analysed the velocity of H I absorption features on a Galactic rotation curve model to derive the Wd 1 distance as d = 3.9±0.7 kpc. Other distances were derived through colour-magnitude diagram (CMD) analysis, using isochrone fitting procedures to evaluate the distance modulus for the cluster. Westerlund (1987) reported d = $5.0^{+0.5}_{-1.0}$ kpc, while Piatti et al. (1998) derived d = 1.0±0.4 kpc. Clark et al. (2005) suggested 2 < d < 5.5 kpc through calibrated luminosity of YHG and limiting luminosity for RSGs to be lower than the Humphreys-Davidson limit. The major issue in Clark et al. (2005) distance determinations is related to the assumption of a standard reddening law ($R_V = 3.1$, Cardelli et al. 1989) towards the cluster, in contradiction with their photometry which indicated that OB stars had a non-standard reddening. The minimum distance (2 kpc) was based on the non-detection of radio-emission from WR stars. Crowther et al. (2006) used JHK_s photometry of WR stars obtaining d ~ 5.5 kpc. Their adoption of Indebetouw et al. (2005) reddening law is a weak point

since it does not apply to inner regions of the Galactic plane (see D16). Negueruela et al. (2010) used OB supergiants and isochrone fitting to derive a distance of d ≈ 5 kpc. Despite those results being based on accurate spectral classification of the sources, they have uncertainties from using the Rieke & Lebofsky (1985) reddening law and the assumption those are single stars, while many OB supergiants are probably binaries with similar brightness companions (Crowther et al. 2006; Clark et al. 2019). Gennaro et al. (2011) reported d = 4.0±0.2 kpc based on fit to the isochrones of pre-MS stars. Hosek et al. (2018) obtained d = 4.4±0.3 kpc by fitting the MS assuming an age of 5 Myr. The weakness of the isochrone fitting method is the large degeneracy between extinction and distance, in addition to the strong dependency on the adopted reddening law.

Astrometric studies opened very promising horizons with the Gaia mission. Indeed, astrometric measurements (position, proper motion and parallaxes) are independent of age, extinction and reddening law. Unfortunately, the Gaia performance for objects at distances of ~kpc scales, especially in dusty regions in the Galactic Center direction, is still impacted because parallax zero-points are still uncertain for very red colour indices (Lindegren et al. 2021b). For Wd 1, the systematic effects are also affected by crowding, individual motions within the cluster, and motions due to binary orbits. To test the reliability of the second Data Release of the Gaia mission (Gaia DR2) Aghakhanloo et al. (2020) used Bayesian inference to derive the distance to both the Wd 1 cluster members and the surrounding Galactic field stars, obtaining d = $2.6^{+0.6}_{-0.4}$ kpc for Wd 1. Aghakhanloo et al. (2021) performed a similar study using the Gaia Early Data Release 3 (Gaia-EDR3), obtaining d = $2.8^{+0.7}_{-0.6}$ kpc. Based on the parallax of OB-type stars in the Gaia DR2, Davies & Beasor (2019) reported d = $3.87^{+0.95}_{-0.64}$ kpc. Rate et al. (2020) used a sample of 18 WRs and OB stars present in Gaia DR2 to derive the distance of d ~ 3 kpc. Beasor et al. (2021) used the same method as Davies & Beasor (2019) using Gaia-EDR3 which shows an improved zero-point parallax determination (Lindegren et al. 2021b), reporting the distance of d = $4.12^{+0.66}_{-0.33}$ kpc. In order to maximise cluster membership, they selected OB-type stars within 5′ from the cluster center and excluded stars with proper motions larger than 10 km s^{-1}, which is the approximate Virial velocity for a cluster with 10^5 M$_\odot$ and size of 1 pc. More recently, Negueruela et al. (2022), reported a distance of d = $4.23^{+0.23}_{-0.21}$ kpc based on the astrometry and photometry of the massive stellar population of Wd 1 from Clark et al. (2020).

In this work, we fine-tune procedures to improve the accuracy of the distance determination to the Westerlund 1 cluster using astrometry and photometry from the Gaia-EDR3 cluster members reported by Clark et al. (2020). We also adopt the distance of the W36 binary system from Rocha et al. (2022, hereafter Paper II), $d_{w36} = 4.03 \pm 0.25$ kpc, as an independent distance measurement to confirm the Gaia-EDR3 results.

This manuscript is organised as follows. In Sec. 3, we present the Gaia-EDR3 data used for deriving the distance to the Wd 1 cluster and the JHK_s photometry of the four RSGs. Section 4 presents the main results, including the analysis of the Gaia-EDR3 data and the distance to the Wd 1 cluster, followed by the age determination based on the Red Supergiant stars. We discuss the implications of our results in Section 5, and we summarise our results in Sect. 6.

2 INTRODUCTION

The formation and evolution of massive stars is poorly known because massive stellar clusters are extremely rare within distances that their stellar population can be resolved. In this context, Wester-

lund 1 (henceforth Wd 1) is relevant, since it is potentially the most massive ($\sim 6 \times 10^4\,M_\odot$, Portegies Zwart et al. 2010 and references therein) young stellar cluster (4-11 Myr, Beasor et al. 2021; Brandner et al. 2008; Gennaro et al. 2011) in our Galaxy. It is a local sibling of 30 Dor, although a little denser and less massive than this one. Wd 1 is located at ~ 10 times closer distance (3-5 kpc - Andersen et al. 2017; Kothes & Dougherty 2007; Davies & Beasor 2019; Beasor et al. 2021), making it an ideal template for investigating the massive stellar formation and evolution process in the nearby Universe, but still at a considerable large distance and extinction ($A_V \sim 11.5$, Damineli et al. 2016; Hosek et al. 2018) that precluded its fully characterisation until now. This massive cluster harbours a large population of confirmed massive stars evolved off the Main Sequence (MS): four Red Supergiants (RSG), 24 Wolf-Rayets (WR), more than 100 Blue Giant and Supergiants OB stars, one magnetar, one Luminous Blue Variable (LBV), one B[e], and six Yellow Hypergiants (YHG) - a short-lived phase (Clark et al. 2005; Crowther et al. 2006; Muno et al. 2006; Negueruela et al. 2010). Given its large population of massive stars, Wd 1 is expected to generate more than a thousand supernovae explosions, producing a significant number of X- and γ-rays binaries, and the coalescence of some of them will likely generate gravitational waves (Abbott et al. 2020). Indeed, several X-ray binaries were already identified due to thermal X-rays produced by wind-wind collision in massive binaries (Skinner et al. 2006). The fraction of binaries is still not precisely known but is estimated to be a relatively large fraction of the Wd 1 stellar population ($> 70\%$, Crowther et al. 2006, Clark et al. 2019; $> 40\%$, Ritchie et al. 2021 - submitted)). Binarity among massive stars is relevant since $> 70\%$ of them will exchange mass with the companion, frequently leading to a binary merger (Sana et al. 2012) with potential for producing gravitational waves.

The question of whether Wd 1 serves as a "golden-standard" laboratory for massive stellar evolution (Clark et al. 2014) is still under debate. There is a large age discrepancy between different methods for Wd 1. The pre-MS sequence population indicates an age of ~ 5-7 Myr (Andersen et al. 2017), much younger than that of the less-luminous RSG (~ 11 Myr, Beasor et al. 2021, leaving the door open for more than a unique episode of star formation over time. Since extinction and distance are not well constrained for Wd 1, absolute luminosities are uncertain, impacting the determination of individual stellar ages and, thus, the age of the cluster itself.

The presence of RSGs and WRs in a coeval cluster would indicate a narrow range of possible ages in a scenario of stars evolving in isolation (~ 5 Myr, Clark et al. 2005). However, binary interactions shape the unique cohort of hypergiant stars, with mass-stripped primaries, rejuvenated secondaries, and merger products (Clark et al. 2020). Beasor et al. (2021) proposed that stars in Wd 1 formed over a period of several Myr, similar to R136/NGC 2070, based on the evolved population (Schneider et al. 2018). However, this cluster shows many sub-clusters distributed throughout its confines which does not seem to be the case for Wd 1. The same authors point to the difference between the HRD of Wd 1 and RSGC1 (Davies et al. 2008). Although RSGC1 has a total mass and the age of RSGs similar to those in Wd 1, it does not show any WR and is prone to represent a single starburst.

The reddening law and extinction were accurately determined by Damineli et al. (2016, hereafter D16) using colour indices of bright cluster members calibrated from spectral types reported by Clark et al. (2005); Ritchie et al. (2009); Negueruela et al. (2010); Clark et al. (2020) and JHK_s photometry measurements combining telescopes of different diameters (4-m, 60-cm and mask aperture of 2-cm). Hosek et al. (2018) used JHK_s photometry and

modelled the colour excesses of MS members by adopting a 5 Myr isochrone. They found good agreement between the average extinction to the cluster ($A_{Ks} = 0.78 \pm 0.16$ mag) with that reported by D16 ($A_{Ks} = 0.74 \pm 0.01$ mag). Hosek et al. (2018) also derived a steep optical/NIR reddening law similar to the of D16 and showed that it is not compatible with previous ones, even with those tuned to the inner Galaxy (Galactic Bulge, outside of the Galactic Plane), such as reported by Nishiyama et al. (2009). To date, the reddening law and the mean A_{Ks} extinction are the best well-constrained parameters for the Wd 1 cluster.

Previous distance determinations, however, have not converged to a $\sim 10\%$ accuracy, which is an uncertainty level desired for this case. The first suggestion for the Wd 1 distance was made by Westerlund (1961) by assuming it was located on the Sagittarius arm, at $d > 1.4$ kpc. Kothes & Dougherty (2007) analysed the velocity of H I absorption features on a Galactic rotation curve model to derive the Wd 1 distance as $d = 3.9 \pm 0.7$ kpc. Other distances were derived through colour-magnitude diagram (CMD) analysis, using isochrone fitting procedures to evaluate the distance modulus for the cluster. Westerlund (1987) reported $d = 5.0^{+0.5}_{-1.0}$ kpc, while Piatti et al. (1998) derived $d = 1.0 \pm 0.4$ kpc. Clark et al. (2005) suggested $2 < d < 5.5$ kpc through calibrated luminosity of YHG and limiting luminosity for RSGs to be lower than the Humphreys-Davidson limit. The major issue in Clark et al. (2005) distance determinations is related to the assumption of a standard reddening law ($R_V = 3.1$, Cardelli et al. 1989) towards the cluster, in contradiction with their photometry which indicated that OB stars had a non-standard reddening. The minimum distance (2 kpc) was based on the non-detection of radio-emission from WR stars. Crowther et al. (2006) used JHK_s photometry of WR stars obtaining $d \sim 5.5$ kpc. Their adoption of Indebetouw et al. (2005) reddening law is a weak point since it does not apply to inner regions of the Galactic plane (see D16). Negueruela et al. (2010) used OB supergiants and isochrone fitting to derive a distance of $d \approx 5$ kpc. Despite those results being based on accurate spectral classification of the sources, they have uncertainties from using the Rieke & Lebofsky (1985) reddening law and the assumption those are single stars, while many OB supergiants are probably binaries with similar brightness companions (Crowther et al. 2006; Clark et al. 2019). Gennaro et al. (2011) reported $d = 4.0 \pm 0.2$ kpc based on fit to the isochrones of pre-MS stars. Hosek et al. (2018) obtained $d = 4.4 \pm 0.3$ kpc by fitting the MS assuming an age of 5 Myr. The weakness of the isochrone fitting method is the large degeneracy between extinction and distance, in addition to the strong dependency on the adopted reddening law.

Astrometric studies opened very promising horizons with the Gaia mission. Indeed, astrometric measurements (position, proper motion and parallaxes) are independent of age, extinction and reddening law. Unfortunately, the Gaia performance for objects at distances of $\sim$kpc scales, especially in dusty regions in the Galactic Center direction, is still impacted because parallax zero-points are still uncertain for very red colour indices (Lindegren et al. 2021b). For Wd 1, the systematic effects are also affected by crowding, individual motions within the cluster, and motions due to binary orbits. To test the reliability of the second Data Release of the Gaia mission (Gaia DR2) Aghakhanloo et al. (2020) used Bayesian inference to derive the distance to both the Wd 1 cluster members and the surrounding Galactic field stars, obtaining $d = 2.6^{+0.6}_{-0.4}$ kpc for Wd 1. Aghakhanloo et al. (2021) performed a similar study using the Gaia Early Data Release 3 (Gaia-EDR3), obtaining $d = 2.8^{+0.7}_{-0.6}$ kpc. Based on the parallax of OB-type stars in the Gaia DR2, Davies & Beasor (2019) reported $d = 3.87^{+0.95}_{-0.64}$ kpc. Rate et al. (2020) used a sample of 18 WRs and OB stars present in Gaia DR2 to derive the distance

of d ∼ 3 kpc. Beasor et al. (2021) used the same method as Davies & Beasor (2019) using Gaia-EDR3 which shows an improved zero-point parallax determination (Lindegren et al. 2021b), reporting the distance of d = 4.12$^{+0.66}_{-0.33}$ kpc. In order to maximise cluster membership, they selected OB-type stars within 5′ from the cluster center and excluded stars with proper motions larger than 10 km s^{-1}, which is the approximate Virial velocity for a cluster with 10^5 M$_\odot$ and size of 1 pc. More recently, Negueruela et al. (2022), reported a distance of d = 4.23$^{+0.23}_{-0.21}$ kpc based on the astrometry and photometry of the massive stellar population of Wd 1 from Clark et al. (2020).

In this work, we fine-tune procedures to improve the accuracy of the distance determination to the Westerlund 1 cluster using astrometry and photometry from the Gaia-EDR3 cluster members reported by Clark et al. (2020). We also adopt the distance of the W36 binary system from Rocha et al. (2022, hereafter Paper II), $d_{w36} = 4.03 \pm 0.25$ kpc, as an independent distance measurement to confirm the Gaia-EDR3 results.

This manuscript is organised as follows. In Sec. 3, we present the Gaia-EDR3 data used for deriving the distance to the Wd 1 cluster and the JHK_s photometry of the four RSGs. Section 4 presents the main results, including the analysis of the Gaia-EDR3 data and the distance to the Wd 1 cluster, followed by the age determination based on the Red Supergiant stars. We discuss the implications of our results in Section 5, and we summarise our results in Sect. 6.

3 DATA

3.1 Gaia-EDR3 archive

We downloaded the list containing all sources of the Gaia-EDR3 catalogue within a 15′ radius around the central position of the Wd 1 cluster (RA = 16:47:04.00, Decl. = −45:51:04.9, Clark et al. 2005), and a total of 36,116 sources were found. We kept only sources associated with a Renormalised Unit Weight Error (RUWE) value ≤ 1.4 (for more details on the definition of RUWE, see Lindegren et al. 2018), and those detected above 3-σ in all three photometric bands (BP, G and RP), leading to a final list of 25,501 objects.

The new astrometric solution for Gaia-EDR3 (Lindegren et al. 2021a,b)) divides the sources into three main groups: *a*) "2-p": objects with two parameters solved (i.e. position); *b*) "5-p": five parameters solved (i.e. position, parallax, proper motion); and *c*) "6-p": six parameters solved, including the source colour (effective wavelength) defined as `pseudocolour` in the Gaia catalogue. The 6-p category encompasses the faintest sources, and/or objects with no reliable colour listed in Gaia DR2 (Fabricius et al. 2021). Among the astrometric groups, the 5-p sources exhibit the most accurate astrometric solutions and, therefore, correspond to the best class of objects to investigate regions associated with high-extinction and/or at relatively large distances.

Among the selected 25,501 Gaia-EDR3 objects, 7,736 and 17,765 are associated with 5-p and 6-p astrometric solutions, respectively.

3.1.1 Wd 1 members in the Gaia-EDR3 catalogue

The identification of cluster members in the Gaia-EDR3 catalogue was performed in two steps. First, we identified each member in one of the few catalogues which have been cross-matched with GAIA-DR3, such as the Guide Star Catalog II Lasker et al. (GSC-II 2008) in visible wavelengths, and the Two Micron All Sky Survey Skrutskie et al. (2MASS 2006) in the near-infrared. Then, we cross-matched the GSC-II IDs with the `gsc23_best_neighbour` table of the Gaia-EDR3 catalogue, and the 2MASS IDs with the `tmass_best_neighbour` table. The positions of 166 stellar members of Westerlund 1 reported by Clark et al. (2020) were cross-matched with the GSC-II and the 2MASS catalogues (assuming a maximum offset of 1″), resulting in a list of 85 sources with a 2MASS counterpart and 105 sources with a GSC counterpart.

Then, the lists were cross-matched with the Gaia-EDR3, leading to a final list with 106 Wd 1 members associated with a Gaia-EDR3 counterpart, from which 61 corresponds to 5-p sources (listed in Table A1), 29 sources are 6-p (Table A2), and 16 have Gaia-EDR3 counterparts with no astrometric information. These last 16 objects were merged with 60 other Wd 1 members with no Gaia-EDR3 counterparts (Table A3).

3.1.2 Parallax zero-point correction: the analysis for Wd 1 members

We corrected Gaia-EDR3 parallaxes by using the methodology described in Lindegren et al. (2021b) and implemented in Python[1], which estimates the parallax zero-point (π_{ZP}) separately for 5- and 6-parameter astrometric solutions as a function of the ecliptic latitude (`ecl_lat`), the G-band magnitude (`phot_g_mean_mag`), and the colour (effective wavenumber) for each source. The correction is well-determined for objects exhibiting G-band magnitudes between 6 and 21 mag, and effective wavenumber values between 1.1 and 1.9 for 5-p solutions (`nu_eff_used_in_astrometry`), and between 1.24 and 1.72 for 6-p solutions (`pseudocolour`).

Figure 1 presents the distribution of the G-band magnitude against the effective wavenumber, for the known Wd 1 members classified as 5-p (61 sources, panel a) and as 6-p objects (27, panel b). In Fig. 1 (a), the distribution of the 5-p sources shows that all points are located within the limits for the proper determination of their π_{ZP} values. On the other hand, Fig. 1 (b) shows that all the 6-p sources exhibit pseudocolour values outside the limits for obtaining a proper ZP correction, leading to dubious values.

Figure 2 presents the G-band magnitude versus wavenumber plot exhibiting all the 25,501 sources selected in Sect. 3. From the 7,736 sources with a five astrometric parameter solution (panel a), only two are located outside the ν_{eff} limit (1.1-1.9). However, ∼52% of the 6-p sources (panel b) exhibit pseudocolour values outside of the (1.24-1.72) limit, indicating that about half of the 17,765 sources does not have a reliable parallax zero-point estimate. Given that all the Wd 1 members associated with 6-p solutions do not have reliable parallax zero-point corrections (Fig. 1), we restricted the further analysis and results using only the 5-p sources from the Gaia-EDR3 catalogue, leading to a sample of 61 known Wd 1 members from a total of 7,736 sources.

3.1.3 Selection of new Wd 1 member candidates based on the Gaia-EDR3 information

We used the Gaia-EDR3 astrometry and photometry to select additional Wd 1 member candidates based on the colour indices of the known members selected in Sect. 3.1.1. The main photometric and astrometric properties of the known members of Wd 1 are summarised in Table 2.

The sample exhibits $BP - RP$ colour indices ranging between

---

[1] https://www.cosmos.esa.int/web/gaia/edr3-code

Table 1. List of known Westerlund 1 members with Gaia EDR3 counterparts associated with a 5-parameter astrometric solution (5-p). The full table is available online at the CDS.

Name	GSC designation	2MASS designation	Gaia EDR3 designation	RUWE	π (mas)	π_{ZP} (mas)	μ_α (mas yr^{-1})	μ_δ (mas yr^{-1})	ν_{eff} (μm^{-1})
W2a	–	16465971-4550513	5940106758703247360	0.94	0.264 ± 0.044	-0.068	-2.015 ± 0.053	-3.414 ± 0.045	1.156
W4	S8UV052685	16470142-4550373	5940106763014985088	0.96	0.180 ± 0.059	-0.045	-2.237 ± 0.073	-3.415 ± 0.063	1.136
W5	2MIU38SH	16470298-4550199	5940106797374726784	1.09	0.154 ± 0.056	-0.073	-2.495 ± 0.068	-3.467 ± 0.059	1.151
W6a	2MIU38SN	16470303-4550235	5940106797374726144	1.01	0.249 ± 0.059	-0.076	-2.222 ± 0.071	-3.803 ± 0.062	1.150
W7	S8UV052690	16470363-4550144	5940106793062992128	0.89	0.122 ± 0.059	-0.014	-2.379 ± 0.074	-3.713 ± 0.063	1.131
W8a	S8UV052686	16470480-4550251	5940106041460479488	0.88	0.119 ± 0.061	-0.018	-2.376 ± 0.075	-3.786 ± 0.065	1.129
W10	S8UV052706	16470334-4550346	5940106797366404480	1.00	0.137 ± 0.063	-0.075	-1.989 ± 0.075	-3.421 ± 0.065	1.133
W11	S8UV052697	–	5940106758703254656	0.95	0.144 ± 0.052	-0.071	-2.480 ± 0.064	-4.007 ± 0.056	1.143
W12a	S8UV052692	16470222-4550590	5940106763006638848	1.00	0.154 ± 0.073	-0.006	-2.493 ± 0.088	-3.692 ± 0.076	1.114
W13	S8UV052698	16470646-4550261	5940106037157928064	0.94	0.094 ± 0.052	-0.071	-2.497 ± 0.069	-4.112 ± 0.060	1.147

Notes: The columns are as follows: (1) Name of the source (the coordinates are listed in Clark et al. (2019)); (2) designation of the source in the GSC 2.3 catalogue; (3) designation of the source in the 2MASS PSC catalogue (Skrutskie et al. 2006); (4) Identification of the Gaia EDR3 source; (5) Renormalized Unit Weight Error; (6) Parallax listed from the Gaia EDR3 and its error; (7) Parallax zero-point correction derived from Lindegren et al. (2021b); (8)-(9) Proper motion in RA and Decl axis and their error; (10) ν_{eff}.

Table 2. General properties of the known Wd 1 members in the Gaia-EDR3 catalogue.

Parameter	Min	Max	Median $\pm$ 1-σ
G (mag)	10.94	17.71	$15.18^{+1.35}_{-2.54}$
BP-RP (mag)	3.81	6.87	$4.85^{+0.61}_{-0.39}$
BP-G (mag)	2.32	5.30	$3.26^{+0.59}_{-0.32}$
G-RP (mag)	1.42	1.68	$1.54^{+0.06}_{-0.05}$
RUWE	0.84	1.39	$0.98^{+0.05}_{-0.06}$
π (mas)^a	0.03	0.50	$0.24^{+0.09}_{-0.10}$
μ_α (mas yr^{-1})	-2.65	-1.57	$-2.27^{+0.23}_{-0.23}$
μ_δ (mas yr^{-1})	-4.24	-3.26	$-3.69^{+0.27}_{-0.17}$
μ (mas yr^{-1})	3.91	5.00	$4.33^{+0.15}_{-0.24}$

Notes: The table presents the minimum, the maximum, the median and the $\pm$1-σ deviation from the median values of each parameter. (a) zero-point corrected parallaxes.
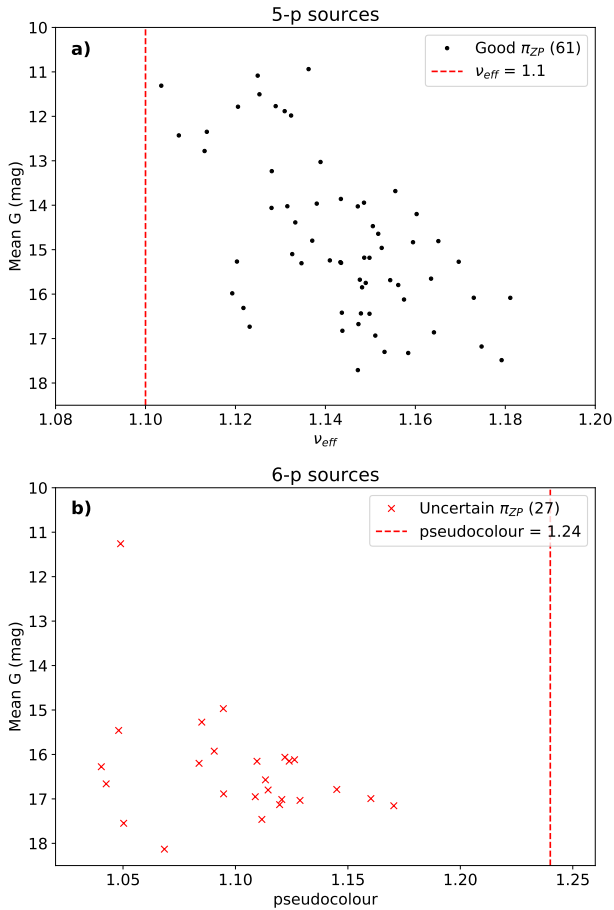
Figure 1. Colour versus G-band mean magnitude for the known Wd 1 members with Gaia-EDR3 counterparts exhibiting five (5-p, panel a) and six astrometric parameters solved (6-p, panel b). Black points indicate the objects with a reliable parallax zero-point correction, while red × symbols indicate sources located outside the limits for the correction. The vertical dashed lines are placed at $\nu_{eff} = 1.1$ (a) and pseudocolour = 1.24 (b).

3.8 and 6.9 mag with a median of $4.9^{+0.6}_{-0.4}$ mag, suggesting a relatively high reddening towards the cluster. For completeness, the $BP - G$ colour index ranges from 2.3 to 5.3 mag with a median of $3.3^{+0.6}_{-0.3}$ mag, and the $G - RP$ colour index ranges from 1.4 to 1.7 mag with a median of $1.54^{+0.06}_{-0.05}$ mag.

We defined three photometric criteria to select new candidates based on the minimum colour indices of the Wd 1 members:

$$BP - RP \geq 3.60 \tag{1}$$

$$BP - G \geq 2.20 \tag{2}$$

$$G - RP \geq 1.35 \tag{3}$$

An additional astrometric criterion was defined by adopting a 5-σ threshold on the two-dimensional proper motion space, filtering out objects with tangential velocities larger than ~30 km s^{-1} at a distance of ~4.0 kpc from the median velocity of the cluster members (see Table 2.

The individual astrometric and photometric criteria led to samples of 1691 and 338 sources, respectively, showing that the photometric criteria are more effective for selecting the new candidates than the astrometric criterion alone. The combination of both selection criteria led to a sample of 166 new objects.

We computed the radial distribution of the density of sources and the median parallax in concentric rings from the center of the
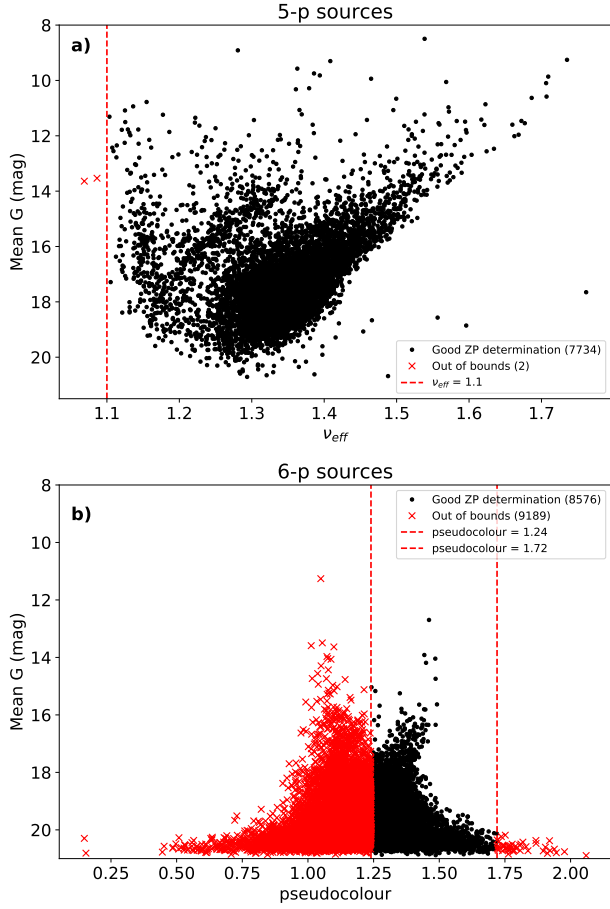
Figure 2. Similar as Fig. 1 but exhibiting all the Gaia-EDR3 sources with five (5-p, panel a) and six astrometric parameters solved (6-p, panel b) within a 15′ radius centered at RA = 251.767°, Dec = −45.849°. The vertical dashed lines are placed at $\nu_{eff} = 1.1$ (a) and pseudocolour = 1.24 and 1.72 (b).

Figure 3. Radial profiles for the median parallax (panel a) and stellar density (panel b) as a function of the distance to the center of the Wd 1 cluster for the initial list of Gaia-EDR3 sources (filled grey curve and + symbols), the Wd 1 members (filled red curve and ∗ symbols), the joint list of candidates and known members (filled green curve and circles), and the field stars (dashed black line). Each value was evaluated in rings of 0.5 for the inner 5′ radius, and 1.0 for r > 5′. The vertical filled and dashed green lines are placed at the effective radius containing about 50% of the cluster population ($R_{50\%}$) and at $3 \times R_{50\%}$.

Wd 1 cluster for the distinct samples. Figure 3(a) shows the radial profile of the stellar density as a function of the distance from the center of the Wd 1 cluster. The initial list of Gaia objects (in grey) exhibits a peak at the central position of FOV (r = 0.5), decreasing towards larger radii. We used the sample containing the candidates and known Wd 1 members (in green) to estimate the effective radius of the cluster ($R_{50\%}$), defined as the radius containing about 50% of the sample, leading to $R_{50\%} = 2.0$ (shown as the vertical filled green line). The known Wd 1 members from Clark et al. (2020) (in red) are found within the inner 5′ radius, which is about $3 \times R_{50\%} = 6.0$ (shown as the vertical dashed green line) containing about ∼75% of the cluster members (known members and candidates, shown by the green curve).

Figure 3(b) exhibits the median parallax as a function of the distance to the center of the cluster for the same samples presented in Fig. 3(a). The curve containing all Gaia-EDR3 sources (filled grey curve) shows an abrupt increase of the median parallax (from $\pi \sim 0.20$ to ∼0.50 mas) in the inner 3′ radius, reaching a roughly constant value for larger radii. The median parallax of the full Gaia-EDR3 sample is strongly biased by the relatively large fraction of Wd 1 members at the central region of the cluster ($r \sim 0'$), while the bias diminishes towards larger distances. The r < 3.0 limit is roughly consistent with the effective radius of the cluster defined in
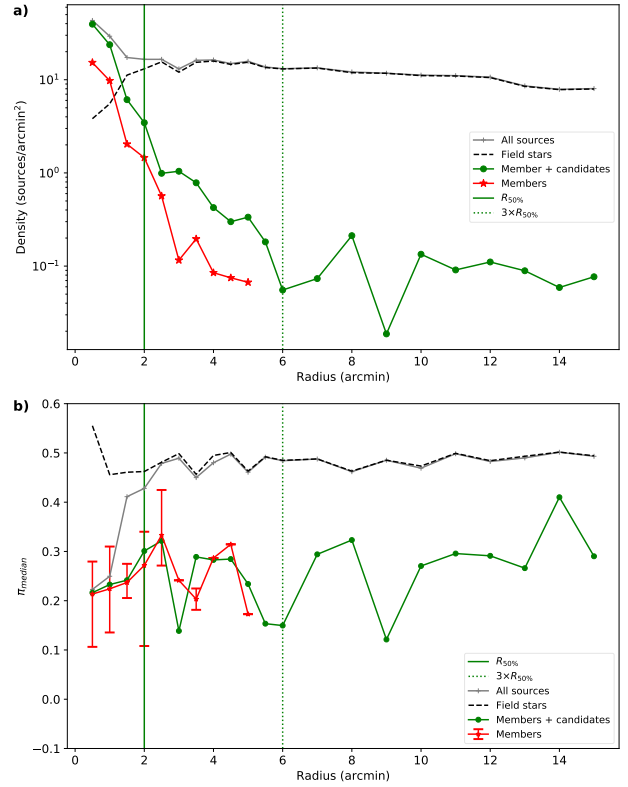
Fig. 3(a), indicating that most of the stellar sources located within this radius are likely members of the cluster. As expected, the median parallax values for the known Wd 1 members (red curve) are significantly smaller, assuming values ranging from 0.17 to 0.3 mas within the inner 5′ radius. The median parallax values of the cluster members (known members and candidates, in green) exhibit a smooth increase towards distances larger than the $3\,R_{50\%}$ limit (vertical dashed green line), suggesting the existence of another population of stellar objects with similar astrometric and photometric properties as the Wd 1 cluster, but likely not bound to the cluster itself. For this reason, we excluded the sources located at distances larger than 6′, leading to a final sample of 172 sources, from which 111 are not present in the Clark et al. (2020) catalogue.

For completeness, the median parallax values of the field stars (dashed black curve) exhibit a relatively constant value around 0.5 mas within the entire range shown in the plot, indicating that the selection criteria adopted in this work were efficient to select the Wd 1 members even at the innermost region of the cluster.

3.2 Near-infrared photometry and far–red spectroscopy

Photometric JHK_s observations of the Wd 1 cluster were performed at the 60-cm Zeiss telescope of the *Obsevatório Pico dos Dias* (OPD/LNA, Brazil) on 2009-June-18. To avoid saturation with the minimum exposure time, the K_s-band filter was replaced by a narrow filter at $\lambda\,2.14\,\mu$m as a proxy for the K_s filter. In addition to this flux reduction setup, a black cardboard mask was placed in front of the telescope, on which four holes of 2×2 cm were cut. A range of exposure times from 1 to 100 secs were used with and without the mask to sample the bright- and faint-end stars in the field. Additional images without mask were taken to reach a fainter magnitude limit ($K_s \sim 16$).

Optical spectroscopy observations ($\lambda 8400$–8900Å, R$\sim$12,000) of the RGB stars were taken between 2012 and 2014 at OPD, and in 2017 at the SOAR telescope (R$\sim$6,000). We used results reported by Arévalo (2018) for the spectral types, but we did not assign temperatures with those spectral types as the lines defining them (e.g., TiO) are not formed in the stellar photosphere (Davies et al. 2013).

4 RESULTS

4.1 Gaia-EDR3

4.1.1 Astrometric and photometric properties of the cluster members

Figure 4 presents three colour-magnitude diagrams (CMDs) showing the Gaia-EDR3 sources in the field (in grey), the known Wd 1 members (in red), the sample selected through the astrometric and effective radius criteria only (in blue) and the sample selected using the full selection criteria (in black). The known Wd 1 members are located in a reddened sequence in the CMDs (shown as red $\ast$ symbols), justifying the usage of the photometric criteria (defined in Sect. 3.1.1 and indicated by the red dashed lines) to filter out a larger fraction of blue, foreground objects. For completeness, the sample obtained with the complementary selection criteria (i.e. astrometric and radial distance selection only) still exhibits a large fraction of foreground objects.

In addition, another group of relatively bright and intermediate-reddened objects ($G \gtrsim 17$, $1.5 \le [BP - RP] \le 3.5$) is located between the foreground main-sequence line and the reddened sequence corresponding to the Wd 1 cluster. These objects are detected in all diagrams from Fig. 4 and they are consistent with a foreground red clump population, suggesting the existence of an evolved stellar population in the line-of-sight of the Wd 1 cluster that could introduce a bias on the analysis if not properly taken into account.

We also plotted the reddening vectors derived from the Damineli et al. (2016) extinction law in each of the CMDs from Fig 4. The extinction coefficients were obtained for each Gaia filter assuming the following effective wavelengths of 532, 673, and 797 nm for the BP-, G-, and RP-bands, respectively (Jordi et al. 2010).

Figure 5 exhibits the distribution of each sample in the proper motion space. The proper motion of the known Wd 1 members (in red) range $-2.65 \le \mu_\alpha \le -1.57$ mas yr^{-1} (median of $-2.26^{+0.28}_{-0.23}$ mas yr^{-1}) and $-4.24 \le \mu_\delta \le -2.39$ mas yr^{-1} (median of $-3.69^{+0.24}_{-0.17}$ mas yr^{-1}). The 1-σ values correspond to a velocity dispersion of about ± 5. km s^{-1} at a distance of ~ 4 kpc. The 5-σ confidence interval ellipsoid for the proper motions of the known Wd 1

members, shown as the red curve in Fig. 5, was used as the astrometric selection criterion defined in Sect. 3.1.1. The ellipsoid is based on the covariance matrix and the linear Pearson correlation coefficient of the two-dimensional data (that is, μ_α versus μ_δ), and the size of the ellipsoid is defined as the number of standard deviations (σ) of the distribution.

The known Wd 1 members (in red) exhibit a compact distribution in terms of proper motions, as expected for a cluster of stars. The Wd 1 members also lie inside the 1-σ confidence interval of the initial list (indicated by the dashed grey curve). The center of the distribution of the members is offset by $(-0.49, -0.29)$ mas from the center of the initial list of Gaia-EDR3 sources, corresponding to a linear projected velocity of about ~ 10 km s^{-1} at a distance of ~ 4.0 kpc. About half of the sample selected through the photometric and angular distance criteria defined in Sect. 3.1.1 are located within the 5-σ confidence interval of the known members (dashed red curve), leading to the final list of 111 new Wd 1 member candidates.

Figure 6 presents the distribution of the parallax values for the initial list of Gaia-EDR3 sources (in grey), the known Wd 1 members (in red), the samples selected through angular distance and effective radius (yellow), astrometric (green) and photometric criteria (blue), and the known cluster members + candidates (in black). As expected, the selection criteria applied to the Gaia-EDR3 sources was efficient to filter out objects associated with large parallax values (e.g. at closer distances), leading to a final sample exhibiting a relatively narrow distribution of parallaxes with a median value around 0.25 mas (indicated by the vertical black line). The resulting distribution is in good agreement with the value observed for the known Wd 1 members (0.236 mas, shown as the vertical red line).

Figure 7 exhibits the spatial distribution of the sources in the FOV. As expected, the Wd 1 members and the new candidate Wd 1 members (shown as red *ast* and black circle symbols, respectively) exhibit a cusp distribution around the central position of Wd 1 in both axis. The sources selected through the photometric criteria alone (in blue) exhibits a tailed distribution extending to $\sim 12'$ to the West direction of Wd 1, while about 20 sources are located at r > 10' the SE direction of the cluster. These objects exhibit similar colours as the cluster members and are likely located at the same distance (i.e. the same spiral arm) as the cluster itself.

4.1.2 Distance inference from the Gaia-EDR3 parallaxes

We followed the methodology of Cantat-Gaudin et al. (2018) to infer the distance to the Wd 1 cluster based on the parallax values (π) and their uncertainties (σ_π) of selected members, computing the distance to the cluster (d) through a maximum likelihood procedure defined as:

$$\prod_{i=1}^{n} P(\pi_i | d, \sigma_{\pi_i}) = \prod_{i=1}^{n} \frac{1}{\sqrt{2\pi\sigma_{\pi_i}^2}} \exp\left(-\frac{(\pi_i - 1/d)^2}{2\sigma_{\pi_i}^2}\right) \qquad (4)$$

As pointed out by those authors, this method does not take into account the physical depth of the cluster neither the position of the sources within the cluster, assuming that all members are located at the same distance. This approximation is true for distant clusters, from which the physical depth is relatively small when compared to the individual parallax uncertainties of its members. To verify if such approximation is valid for Wd 1, Fig. 8 shows the ratio between the parallax and their errors (π/σ_π) as a function of the G-band magnitude of the Gaia-EDR3 sources. The plot exhibits a large fraction of the selected Wd 1 sources (red $\ast$ symbols) associated with
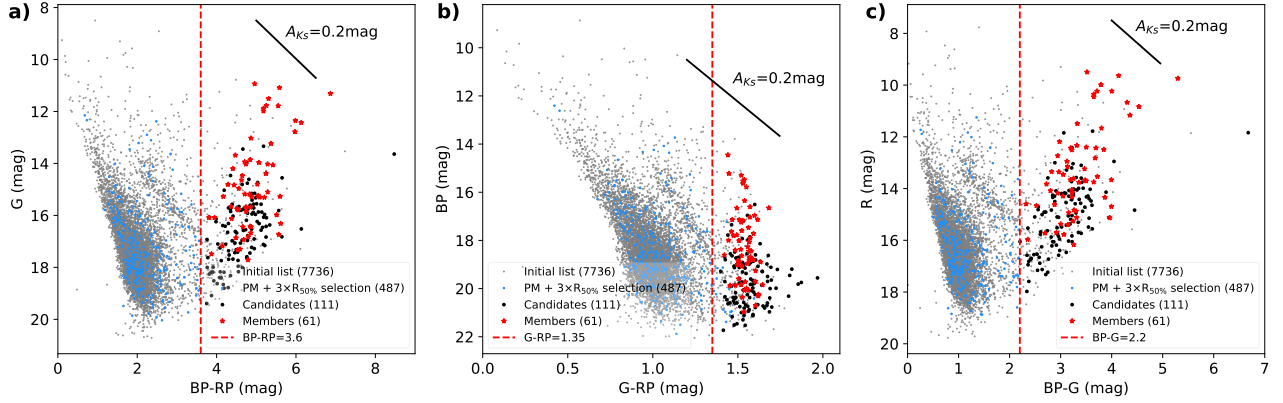
Figure 4. Colour-magnitude diagrams using the photometry of Gaia-DR3 sources within a 15′ radius around the Wd 1 central position. The initial list of Gaia-EDR3 sources is indicated by grey circles, known Wd 1 members are shown as red * symbols, sources selected using the astrometric and effective radius criteria are shown as blue circles, and the Wd 1 member candidates are shown as black circles. The vertical dashed red lines indicate the photometric criteria adopted in this work. The black lines illustrate the reddening vectors corresponding to an $A_{Ks} = 0.2$ mag using the extinction law from Damineli et al. (2016).
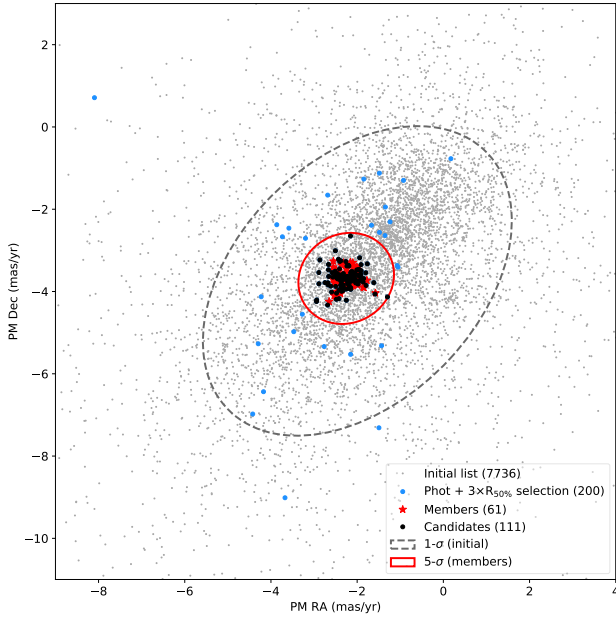

Figure 5. Distribution of the proper motions of the Gaia-EDR3 sources. The initial list of Gaia objects are indicated by filled grey circles, the known Wd 1 members are shown as red * symbols, the sources selected through the photometric and effective radius criteria are shown as filled blue circles and the final sample of Wd 1 member candidates are indicated by filled black circles. The 5-σ confidence interval ellipsoid of the known Wd 1 members (filled red curve) was used to filter out sources with large proper motions. For comparison, the 1-σ confidence interval ellipsoid of the initial list is indicated by the dashed grey curve.

Figure 6. Distribution of the parallax values for the Gaia-DR3 sources. The initial Gaia-EDR3 sample is indicated as grey, known Wd 1 members are shown in red, sources selected through effective radius, astrometric, and photometric criteria are shown as yellow, green and blue, respectively. The final sample of member candidates is indicated in black. The vertical lines are placed at the median parallax values of each sample.

relatively small parallax-to-error ratio values $(0.01 \lesssim \pi/\sigma_\pi \lesssim 10)$ when compared to the values observed for the whole sample of Gaia EDR3 sources in the field (grey points, with π/σ_π values up to $\sim 10^2$). These findings confirm the assumption of large uncertainties on the individual parallaxes of the cluster members and, therefore, its distance can be inferred using Eq. 4.

The result of Eq. (4) is a probability density function (PDF), peaking at the distance where the product $P(\pi|d, \sigma_\pi)$ assumes its

maximum value. The resulting PDF considering the 58 known Wd 1 members is shown as the red curve in Fig. 9. The PDF exhibits an asymmetric profile, with an elongated tail towards large distances. The PDF peaks at the distance of $4.14 \, \text{kpc}^{+0.60}_{-0.66}$ kpc, with the upper and lower uncertainties defined as the 68% confidence interval, consistent with a 1-σ estimate from other methods.

The determination of the distance to the cluster and its associated errors was improved by considering the new Wd 1 member candidates, as shown in Fig. 9. Overlaid on the PDF of the known Wd 1 members (in red), the plot also shows the PDF considering only the new candidates (in blue), and the union of both samples (members + candidates, in black). The sample of 172 objects led to a more precise inference of the distance to the cluster, estimated as $d_{\text{gedr3}} = 4.06^{+0.36}_{-0.34}$ kpc.

For completeness, we computed the weighted-mean parallax of the field stars to infer their mean distance. The weighted mean parallax $(\langle \pi \rangle)$ was evaluated using Eqs. (1)-(3) from Navarete et al. (2019), leading to $\langle \pi \rangle = 0.74 \pm 0.20$ mas. We estimated the distance of the field stars by simply inverting their mean parallax and propagating the errors, leading to a mean distance of $1.36^{+0.50}_{-0.29}$ kpc. Such distance is consistent with the location of the near-side of the Carinae arm at the line-of-sight of Wd 1 cluster Reid et al. (2019).
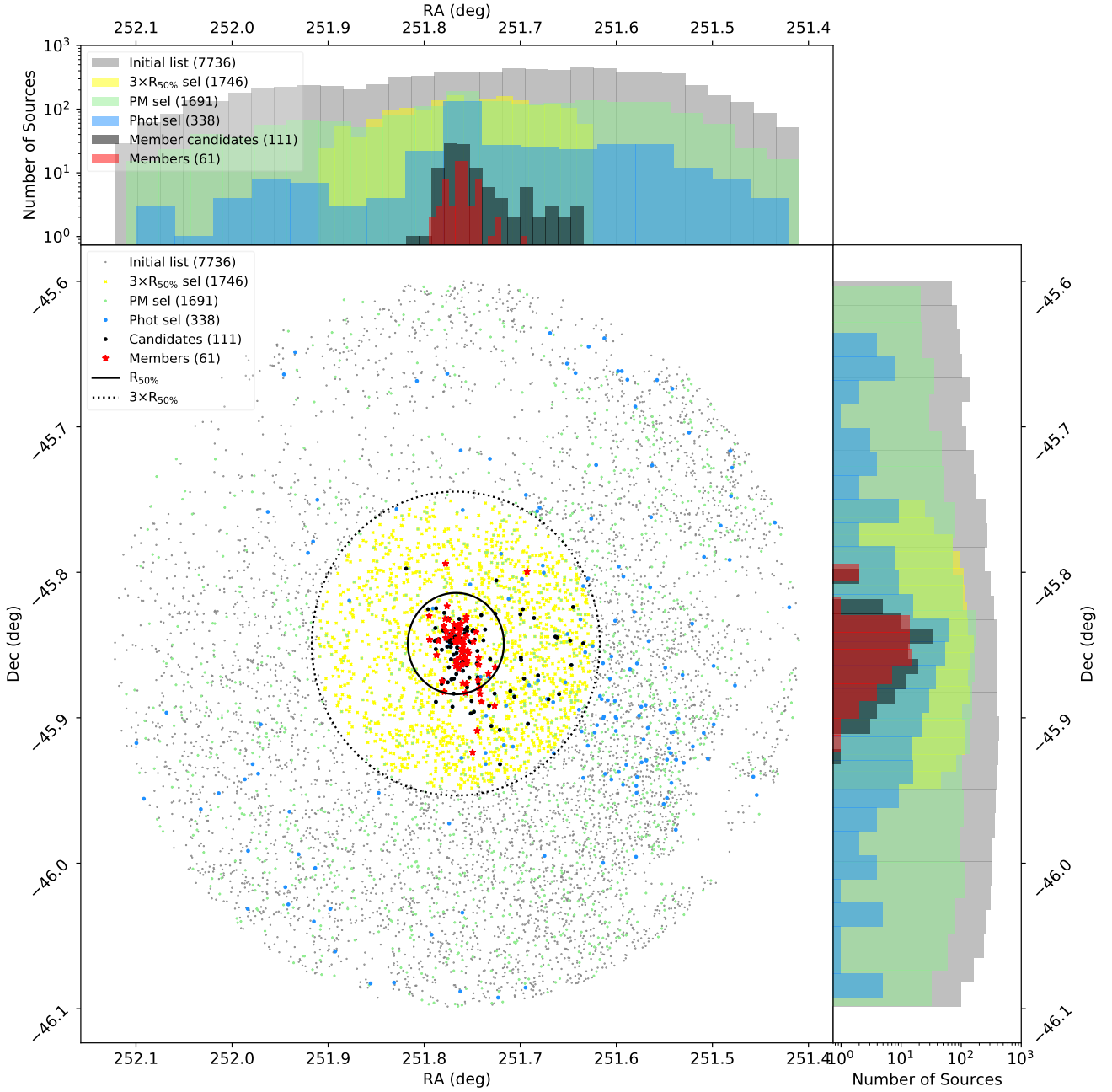
Figure 7. Spatial distribution of the Gaia-EDR3 sources within a radius of 15′ centered at the Wd 1 position (RA = 251.76707°, Dec = −45.84899°). The initial list of Gaia objects are indicated by grey circles, the known Wd 1 members are shown as red ∗ symbols, and the Wd 1 member candidates are indicated by filled black circles. The sub-samples selected through angular distance, astrometric and photometric criteria individually are shown as yellow ×, green +, and blue × symbols, respectively. The top and right panels show the distribution of the same sources as a function of the right ascension and declination, respectively. The effective radius containing 50% of the cluster population ($R_{50\%} = 2′$) and the $3 \times R_{50\%}$ radius are indicated by the filled and dotted black curves, respectively.

A study of the W36 eclipsing binary system (Paper II) led to a independent distance estimate of $d_{w36} = 4.03 \pm 0.25$ kpc, in agreement with our Gaia-EDR3 results. From here on we adopt the weighted mean distance to the cluster as $d_{wd1} = 4.05 \pm 0.20$ kpc (further discussions are presented in Sect. 5.1).

4.2 Luminosity and Age of the Red Supergiants

The improved accuracy of extinction and the distance obtained in this work has a direct impact on the determination of the luminosities of the cluster members. As a consequence, the parameters of the cluster as a whole can also be inferred with greater confidence.

The photometric results for the four RSGs and six YHGs are listed in Table 3. The photon statistics accuracy is ∼0.01 mag for the bright members (degrading for the fainter members), but due
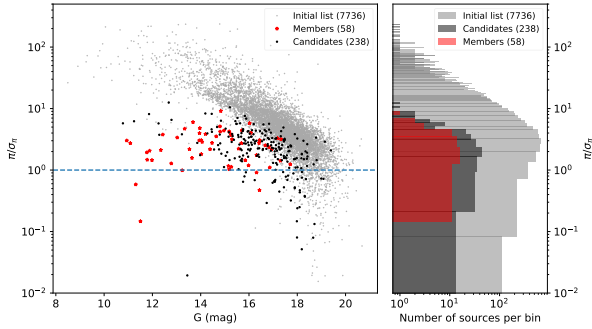
Figure 8. Left panel: Distribution of the parallax-to-error ratio as a function of the G-band magnitude of the Gaia sources. The initial list of Gaia objects are indicated by grey circles, the known Wd 1 members are shown as red $*$ symbols, the new member candidates are indicated by the black circles. The horizontal dashed blue line indicates y = 1. Right panel: distribution of the parallax-to-error ratio values for the three samples. The number of sources per bin increases from left to right.

Figure 9. Probability density function of the posterior distance to Wd 1 based on the known members of the cluster (in red), the selected candidates (in blue), and the union of both samples (in black). The most likely distance of the final sample is $4.06^{+0.36}_{-0.34}$ kpc, indicated by the filled black line, and the 1-σ errors (68%) are shown as dashed black lines. The distances based on the other samples are indicated by the vertical filled lines. The distan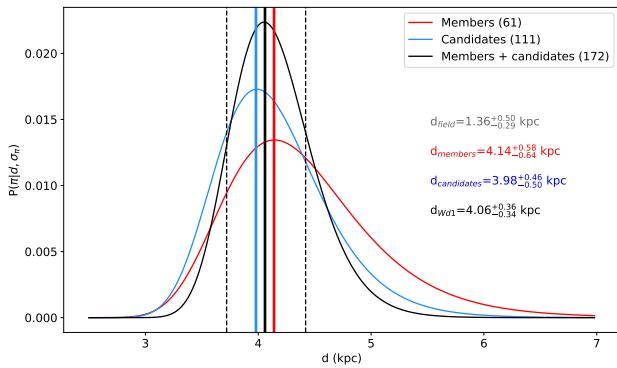ces are listed in their corresponding colours and the distance to the field-stars (not shown in the plot) is listed in grey.

to the relatively small number of 2MASS calibrating sources in the FOV, the photometric accuracy was limited to ∼ 0.05 mag in the bright-end ($K_s < 13$). Using the references in the caption of Table 3 we derived the intrinsic colours and temperatures of our targets. We adopted the Damineli et al. (2016) reddening law to get the AK_s extinction: $AK_s = 0.449E_{J-K_s}$ and $AK_s = 1.300E_{H-K_s}$ (column 6 in their Table 3). The average extinction of the RSGs and YHGs $A_{K_s} = 0.80 \pm 0.14$ is compatible with that derived from the OB stars ($A_{K_s} = 0.74 \pm 0.08$, D16), indicating that these evolved cool stars do not have significant circumstellar extinction. The exception is W75 (in addition to W8a) which has a significantly larger than the average extinction, as suspected by Beasor et al. (2021).

The total luminosity of each RSG (column 7 of Table 3) was calculated by using the bolometric calibration suggested by Davies & Beasor (2018) – $BC_K = 3.00 \pm 0.18$ – and the mean distance of $d_{\rm wd1} = 4.05$ kpc from Sect. 4.1.2. The range of RSGs luminosities is relatively narrow ($\Delta (\log(L/L_\odot) = 0.24$) indicating a narrow range of RSG progenitor masses. Column 8 of Table 3 shows luminosities

from Beasor et al. (2021) (their Table 4, column 6), scaled with our distance of $d = 4.05$ kpc. The results are in excellent agreement in luminosity indicating that the differences between the two works mostly arise from the AK_s extinction towards individual targets.

Table 3 also displays our photometric results for the six YHGs. The bolometric correction follows Flower (1996). Our results are in very good agreement with those reported by Beasor et al. (2021), which is based on independent photometry.

We adopted the *Binary Population and Spectral Synthesis* method (BPASS, Eldridge et al. 2020) for estimating the age based on the mean of the luminosity of the four RSGs (interpolated into their $Z = 0.020$ models, column 6 of Table 1). The mean RSG luminosity, $\log(L_{\rm RSG}/L_\odot) = 5.10 \pm 0.11$ corresponds to a cluster age of 10.7 ± 1 Myr.

5   DISCUSSION

5.1   The distance to Wd1 confirmed by independent methods

We used the Gaia-EDR3 analysis to infer the distance to the Westerlund 1 cluster based on the sample of evolved, high-mass stars from Clark et al. (2020). We further included additional member candidates selected through astrometric and photometric criteria to obtain a final sample of 172 sources with Gaia-EDR3 counterparts, leading to the distance of $d_{\rm gedr3} = 4.06^{+0.36}_{-0.34}$ kpc.

We also found that the sources in Clark et al. (2020) are relatively red objects, as expected for a cluster located at large distances in the Galactic Plane. The main impact of that fact is regarding the parallax zero-point derivation. For the range of brightness and colours of the cluster members in the Gaia-EDR3 catalogue, we found that the parallax zero-point correction is well-determined for Gaia objects with five astrometric parameters solution (5p), but not for objects with six astrometric parameters solution (6p, see Figs. 1 and 2). Therefore, we excluded the 6p sources from our analysis. This criterion was fundamental for removing any systematic biases due to dubious parallax zero-points, a critical correction for objects at relatively large distances.

Our Gaia-EDR3 distance to Wd 1 is in excellent agreement with the distance reported by Beasor et al. (2021), $4.12^{+0.66}_{-0.33}$ kpc. The major difference between their results and ours is mainly related to the sample selection and the adoption of fine-tuning procedures in this work for excluding sources with unreliable zero-point parallax correction (see Sect. 3.1.2).

Negueruela et al. (2022) reported an independent confirmation of the distance to Wd 1 also based on the OB stellar population from Clark et al. (2020). They reported eight distance estimates (see their Table 1), adopting case C as the distance to the cluster, $4.23^{+0.23}_{-0.21}$ kpc. Interestingly, cases F and H of their Table 1 are very similar to our results (their source selection criteria for case H likely match the same as adopted by us). However, apparently they chose case C as an intermediate value of the eight cases instead, stating that their distance estimate is robust and independent in terms of their source selection methodology, the parallax zero-point correction or choice of sources with 5- or 6-parameters astrometric solutions. Taking into account the independent distance of W36 in Paper II ($d_{\rm w36} = 4.03 \pm 0.25$ kpc), the closest distances reported in their Table 1 (cases F, H) are likely more reliable. They adopted a distinct parallax zero-point correction and a specific distance prior for the distribution of OB stars in the Galactic plane (see references therein), which led to a distance in agreement with our results and with those from Beasor et al. (2021).

Table 3. Classification, JHK_s photometry, reddening and bolometric luminosities for Red Supergiants (first four) and Yellow Hypergiants (last six).

ID	Spectral Type	$\log(T_{\rm eff})$	J	H	K_s	A_{Ks}	$\log(L/{\rm L}_\odot)^{\rm a}$	B21[b]
Red Supergiants:								
W237	M3-4 I	-	4.86	3.33	2.44	0.67 ± 0.16	5.21 ± 0.03	5.30
W20	M3-4 I	-	6.28	4.33	3.24	0.95 ± 0.17	4.98 ± 0.03	5.16
W75	M1 Ia	-	6.96	4.68	3.44	1.23 ± 0.15	5.00 ± 0.03	4.90
W26	M1-1.5 Ia	-	4.92	3.16	2.40	0.68 ± 0.02	5.20 ± 0.03	5.45
Yellow Hypergiants:								
W4	F3 Ia+	3.81	6.06	4.92	4.45	0.58 ± 0.15	4.96 ± 0.03	5.04
W8a	F8 Ia+	3.72	6.50	5.41	3.82	1.05 ± 0.20	5.17 ± 0.03	4.73
W32	F5 Ia+	3.79	5.69	4.49	3.87	0.72 ± 0.17	5.17 ± 0.03	5.21
W16a	A5 Ia+	3.91	6.55	5.37	4.78	0.74 ± 0.16	5.28 ± 0.03	4.95
W12a	F1 Ia+	3.83	6.73	5.50	4.84	0.79 ± 0.18	4.97 ± 0.03	4.88
W265	F1-5 Ia+	3.82	6.74	5.45	4.75	0.82 ± 0.16	4.94 ± 0.03	4.88

Notes: (*a*) Spectral Types of RSGs and YHGs from Arévalo (2018) and Clark et al. (2020), respectively, $BC_K = 3.00$ (Davies & Beasor 2018), NIR colours (Koornneef 1983); BC_V (Flower 1996). (*b*) Bolometric luminosities from Beasor et al. (2021, Table 4) scaled to **4.05 kpc**.

Table 4. Gaia-EDR3 distances to Wd 1 reported in the literature and results obtained in Paper I (this work) and Paper II.

Method	Distance (kpc)	Reference
Gaia-EDR3	$4.12^{+0.66}_{-0.36}$	Beasor et al. (2021)
Gaia-EDR3	$4.23^{+0.23}_{-0.21}$	Negueruela et al. (2022)
Gaia-EDR3	$4.06^{+0.36}_{-0.34}$	Paper I (this work)
W36 ecl. binary	4.03 ± 0.25	Paper II

These three Gaia-EDR3 distances indicate that the Wd 1 cluster is located between 4.0 and 4.3 kpc with unprecedented accuracy. In addition, the Gaia-EDR3 distances can be confirmed by independent measurements, such as the modelling of eclipsing binary systems. Indeed, Paper II presents the modelling of the eclipsing binary system W36, obtaining a distance of $d_{\rm w36} = 4.03 \pm 0.25$ kpc. The distance to W36 is consistent within 1-σ with each of the three independent Gaia-EDR3 distances, being an important result once the parallax zero-point corrections are uncertain in the Gaia-EDR3 for most of objects associated with very red colour indices (Lindegren et al. 2021b), as likely observed for the bulk of the Wd 1 cluster members (see Sect. 3.1.2).

Table 4 summarises the distances reported by Beasor et al. (2021), Negueruela et al. (2022), Paper I (this work), and also includes the distance to the massive binary system W36 from Paper II.

At the distance of 4.05 ± 0.20 kpc, the effective size of Wd 1, $r = 2'.0$ (Figs. 3 and 7) corresponds to a linear radius of 2.33 ± 0.12 pc, and our sample is located within three times the effective radius, 7.0 ± 0.4 pc. It is worth mentioning that our sample is biased towards the high-mass stellar content of the cluster. In general, the low-mass counterparts are likely less gravitationally bound to the cluster, extending to larger distances from the center of the cluster. Both the diameter of the cluster and the low-density halo concept are in agreement with the analysis presented by Negueruela et al. (2022).

Wd 1 is located at the galactic latitude of $\ell = 339°.55$. Based on recent Galactic structure results (Reid et al. 2019), the cluster is located in the line-of-sight of three major galactic spiral arms: the Carina arm at a distance of 0.5 kpc, the Scutum-Crux near arm at 3.5 kpc, and the Norma near arm at 5.5 kpc. Our results suggest that the distance of Westerlund 1 is consistent with the position of the far side of the Scutum-Crux near arm, or even the near side of

the Norma arm. Negueruela et al. (2022) provide strong arguments favouring that the cluster is located within the Norma arm, but further studies are still necessary to confirm the true association of the cluster with one or another spiral arm.

5.2 The Age of Westerlund 1

We further compare our results on the age of Wd 1 with those from Beasor et al. (2021). Those authors tested the robustness of different methods for evaluating the age of the cluster by using a wide range of stellar populations (RSGs, PMS and the eclipsing binary W13). They reported the age of $7.2^{+1.1}_{-2.3}$ Myr for the pre-MS population, while the faintest RSG led to a older age between 9.2-11.7 Myr. Our results for the age of the RSGs based on BPASS models (11 ± 1 Myr, see Sect. 4.2) is in excellent agreement with those authors.

In paper II, we derived the age of the eclipsing binary W36 (using Yusof et al. (2022) evolutionary models) as ~6 Myr. Only the W36B component has a reliable age estimation, since the peeling of external layers of the W36A component shifts its effective temperature to the blue, mimicking an earlier age. Furthermore, the impact of mass accretion onto W36B is low since the mass lost by W36A is mainly through its stellar wind, so the W36B stellar parameters are little affected. The age of W36B is not far from the age limit of W13 (< 5 Myr) reported by Beasor et al. (2021) and also to ~7 Myr suggested by Hosek et al. (2018). Compared to the ages of the RSGs, the much younger W36B and W13 sources are evidence of – at least – two episodes of star formation in the cluster.

6 CONCLUSIONS

Our astrometric and photometric analysis using the Gaia Early Data Release 3 (Gaia-EDR3) resulted in the distance of $d_{\rm gedr3} = 4.06^{+0.36}_{-0.34}$ kpc to the massive stellar cluster Westerlund 1. The agreement between the Gaia-EDR3 distance and the distance of the W36 eclipsing binary system $d_{\rm w36} = 4.03 \pm 0.25$ kpc (Paper II) validates our results and, in particular, the parallax zero-point determination for the reddest Wd 1 members classified as 5-p sources in the Gaia-EDR3 catalogue. The weighted mean distance of both independent estimates led to $d_{\rm wd1} = 4.05 \pm 0.20$ kpc, with a unprecedented error of 5%.

We reported the age of the RSG stars using BPASS models for the average luminosity as 9.7–11.7 Myr, in good agreement with

that of W75 reported by Beasor et al. (2021, 9.2–11.7 Myr) based on a broader range of approaches and a different dataset.

The age of W36B is ∼ 6.5 Myr, is close to the < 5 Myr reported by Beasor et al. (2021) for the binary system W13. These two works indicate a range of star formation in Wd1 of 5–12 Myr, in line with the synthetic cluster calculated by Yusof et al. (2022) combining rotating and non-rotating models with an age spread of 5–10 Myr. Yusof et al. (2022) showed that their result was able to reproduce qualitatively the observed population of RSGs, YHGs, and WRs in Wd 1.

DATA AVAILABILITY

The data sets were derived from observations available in the public domain: https://www.cosmos.esa.int/web/gaia/earlydr3.

Tables 3, A1, A2 and A3 are also available in the CDS.

REFERENCES

Abbott R., et al., 2020, Phys. Rev. Lett., 125, 101102
Aghakhanloo M., et al., 2020, MNRAS, 492, 2497
Aghakhanloo M., et al., 2021, Research Notes of the American Astronomical Society, 5, 14
Andersen M., Gennaro M., Brandner W., Stolte A., de Marchi G., Meyer M. R., Zinnecker H., 2017, A&A, 602, A22
Arévalo A. L. E. R., 2018, Master's thesis, Instituto de Astronomia, Geofísica e Ciências Atmosféricas, University of São Paulo, doi:10.11606/D.14.2019.tde-12092018-161841
Beasor E. R., Davies B., Smith N., Gehrz R. D., Figer D. F., 2021, ApJ, 912, 16
Brandner W., Clark J. S., Stolte A., Waters R., Negueruela I., Goodwin S. P., 2008, A&A, 478, 137
Cantat-Gaudin T., et al., 2018, A&A, 618, A93
Cardelli J. A., Clayton G. C., Mathis J. S., 1989, ApJ, 345, 245
Clark J. S., Negueruela I., Crowther P. A., Goodwin S. P., 2005, A&A, 434, 949
Clark J. S., Ritchie B. W., Najarro F., Langer N., Negueruela I., 2014, A&A, 565, A90
Clark J. S., Ritchie B. W., Negueruela I., 2019, A&A, 626, A59
Clark J. S., Ritchie B. W., Negueruela I., 2020, A&A, 635, A187

Crowther P. A., Hadfield L. J., Clark J. S., Negueruela I., Vacca W. D., 2006, MNRAS, 372, 1407
Damineli A., Almeida L. A., Blum R. D., Damineli D. S. C., Navarete F., Rubinho M. S., Teodoro M., 2016, MNRAS, 463, 2653
Davies B., Beasor E. R., 2018, MNRAS, 474, 2116
Davies B., Beasor E. R., 2019, MNRAS, 486, L10
Davies B., Figer D. F., Law C. J., Kudritzki R.-P., Najarro F., Herrero A., MacKenty J. W., 2008, ApJ, 676, 1016
Davies B., et al., 2013, ApJ, 767, 3
Eldridge J. J., Beasor E. R., Britavskiy N., 2020, MNRAS, 495, L102
Fabricius C., et al., 2021, A&A, 649, A5
Flower P. J., 1996, ApJ, 469, 355
Gennaro M., Brandner W., Stolte A., Henning T., 2011, MNRAS, 412, 2469
Hosek Matthew W. J., et al., 2018, ApJ, 855, 13
Indebetouw R., et al., 2005, ApJ, 619, 931
Jordi C., et al., 2010, A&A, 523, A48
Koornneef J., 1983, A&A, 500, 247
Kothes R., Dougherty S. M., 2007, A&A, 468, 993
Lasker B. M., et al., 2008, AJ, 136, 735
Lindegren L., et al., 2018, A&A, 616, A2
Lindegren L., et al., 2021a, A&A, 649, A2
Lindegren L., et al., 2021b, A&A, 649, A4
Muno M. P., et al., 2006, ApJ, 636, L41
Navarete F., Galli P. A. B., Damineli A., 2019, MNRAS, 487, 2771
Negueruela I., Clark J. S., Ritchie B. W., 2010, A&A, 516, A78
Negueruela I., Alfaro E. J., Dorda R., Marco A., Maíz Apellániz J., González-Fernández C., 2022, arXiv e-prints, p. arXiv:2204.00422
Nishiyama S., Tamura M., Hatano H., Kato D., Tanabé T., Sugitani K., Nagata T., 2009, ApJ, 696, 1407
Piatti A. E., Bica E., Claria J. J., 1998, A&AS, 127, 423
Portegies Zwart S. F., McMillan S. L. W., Gieles M., 2010, ARA&A, 48, 431
Rate G., Crowther P. A., Parker R. J., 2020, MNRAS, 495, 1209
Reid M. J., et al., 2019, ApJ, 885, 131
Rieke G. H., Lebofsky M. J., 1985, ApJ, 288, 618
Ritchie B. W., Clark J. S., Negueruela I., Crowther P. A., 2009, A&A, 507, 1585
Rocha D. F., Almeida L. A., Damineli A., Navarete F., et al., submitted 2022, Distance and age of the massive stellar cluster Westerlund 1. II. Eclipsing binary method
Sana H., et al., 2012, Science, 337, 444
Schneider F. R. N., et al., 2018, A&A, 618, A73
Skinner S. L., Simmons A. E., Zhekov S. A., Teodoro M., Damineli A., Palla F., 2006, ApJ, 639, L35
Skrutskie M. F., et al., 2006, AJ, 131, 1163
Westerlund B., 1961, AJ, 70, 57
Westerlund B. E., 1987, A&AS, 70, 311
Yusof N., et al., 2022, MNRAS,

APPENDIX A: FULL TABLES

Table A1. List of known Westerlund 1 members with Gaia EDR3 counterparts associated with a 5-parameter astrometric solution (5-p). This table is available online at the CDS.

Name	GSC designation	2MASS designation	Gaia EDR3 designation	RUWE	π (mas)	π_{ZP} (mas)	μ_α (mas yr^{-1})	μ_δ (mas yr^{-1})	ν_{eff} (μm^{-1})	min(σ_{phot}) (σ)	G (mag)	BP (mag)	RP (mag)
W2a	–	16465971-4550513	5940106758703247360	0.94	0.264 ± 0.044	−0.068	−2.015 ± 0.053	−3.414 ± 0.045	1.156	115.2	13.7	16.7	12.2
W4	S8UV052685	16470142-4550373	5940106763014985088	0.96	0.180 ± 0.059	−0.045	−2.237 ± 0.073	−3.415 ± 0.063	1.136	99.5	10.9	14.5	9.5
W5	2MIU38SH	16470298-4550199	5940106797374726784	1.09	0.154 ± 0.056	−0.073	−2.495 ± 0.068	−3.467 ± 0.059	1.151	87.8	14.5	17.6	12.9
W6a	2MIU38SN	16470303-4550235	5940106797374726144	1.01	0.249 ± 0.059	−0.076	−2.222 ± 0.071	−3.803 ± 0.062	1.150	68.9	15.2	18.4	13.6
W7	S8UV052690	16470363-4550144	5940106793062992128	0.89	0.122 ± 0.059	−0.014	−2.379 ± 0.074	−3.713 ± 0.063	1.131	109.2	11.9	15.5	10.4
W8a	S8UV052686	16470480-4550251	5940106041460479488	0.88	0.119 ± 0.061	−0.018	−2.376 ± 0.075	−3.786 ± 0.065	1.129	134.1	11.8	15.5	10.4
W10	S8UV052706	16470334-4550346	5940106797366404480	1.00	0.137 ± 0.063	−0.075	−1.989 ± 0.075	−3.421 ± 0.065	1.133	80.6	14.4	18.1	12.8
W11	S8UV052697	–	5940106758703254656	0.95	0.144 ± 0.052	−0.071	−2.480 ± 0.064	−4.007 ± 0.056	1.143	144.8	13.9	17.2	12.3
W12a	S8UV052692	16470222-4550590	5940106763006638848	1.00	0.154 ± 0.073	−0.006	−2.493 ± 0.088	−3.692 ± 0.076	1.114	68.1	12.3	16.7	10.7
W13	S8UV052698	16470646-4550261	5940106037157928064	0.94	0.094 ± 0.052	−0.071	−2.497 ± 0.069	−4.112 ± 0.060	1.147	79.4	14.0	17.2	12.5
W16a	S8UV052691	16470661-4550422	5940106041460473216	0.89	0.097 ± 0.066	−0.018	−2.130 ± 0.086	−3.760 ± 0.072	1.121	71.1	11.8	15.8	10.2
W21	2MIU38V7	16470110-4551135	5940106659935758976	0.96	0.296 ± 0.058	−0.077	−2.517 ± 0.081	−3.582 ± 0.062	1.137	55.1	14.8	18.3	13.2
W23a	2MIU38UU	16470256-4551088	5940106758703255168	0.99	0.163 ± 0.054	−0.074	−2.317 ± 0.072	−3.298 ± 0.058	1.132	78.0	14.0	17.7	12.4
W24	2MIU38V4	16470215-4551126	5940106758709795712	0.90	0.212 ± 0.055	−0.079	−2.367 ± 0.073	−3.630 ± 0.060	1.141	61.5	15.2	18.7	13.7
W26	S8UV052688	16470540-4550367	5940106041452150272	1.09	0.053 ± 0.092	−0.024	−1.841 ± 0.127	−3.909 ± 0.108	1.104	21.7	11.3	16.6	9.7
W32	–	16470369-4550435	5940106763006654208	1.00	0.190 ± 0.070	−0.034	−2.262 ± 0.087	−3.615 ± 0.074	1.125	119.8	11.1	15.2	9.6
W33	S8UV052689	16470413-4550485	5940106002789009536	0.84	0.085 ± 0.059	−0.011	−2.053 ± 0.078	−3.728 ± 0.063	1.132	131.5	12.0	15.6	10.5
W35	2MIU38TW	16470417-4550533	5940106007100789760	1.03	0.201 ± 0.064	−0.078	−2.088 ± 0.086	−3.862 ± 0.069	1.143	56.6	15.3	18.8	13.7
W42a	S8UV052694	16470325-4550522	5940106763006644096	0.90	0.092 ± 0.072	−0.018	−1.970 ± 0.091	−3.502 ± 0.078	1.113	85.2	12.8	17.1	11.2
W47	2MIU38VF	16470260-4551177	5940106763014970624	1.32	0.203 ± 0.074	−0.078	−2.649 ± 0.094	−4.242 ± 0.079	1.154	39.2	15.7	18.9	14.1
W52	2MIU397M	16470184-4551294	5940106659927373056	1.03	0.269 ± 0.056	−0.072	−2.140 ± 0.070	−3.873 ± 0.060	1.138	134.0	14.0	17.5	12.4
W54	S8UV051192	–	5940106007092338176	1.05	0.131 ± 0.067	−0.080	−2.244 ± 0.083	−3.801 ± 0.069	1.133	56.1	15.1	18.8	13.5
W55	S8UV051040	16465841-4551313	5940106655624021632	0.99	0.172 ± 0.049	−0.073	−2.333 ± 0.064	−3.849 ± 0.052	1.152	103.9	14.6	17.8	13.1
W57a	S8UV051189	16470136-4551456	5940106655624023552	0.95	0.203 ± 0.060	−0.051	−2.251 ± 0.075	−3.448 ± 0.061	1.139	43.7	13.0	16.4	11.5
W60	S8UV050868	–	5940105904013098496	0.97	0.157 ± 0.055	−0.078	−2.141 ± 0.070	−3.658 ± 0.058	1.143	48.7	15.3	18.6	13.8
W63a	S8UV050867	–	5940105904021499776	0.97	0.118 ± 0.054	−0.076	−2.061 ± 0.067	−3.376 ± 0.056	1.163	37.5	15.7	18.5	14.1
W65	S8UV050871	–	5940105904013103744	0.86	0.196 ± 0.056	−0.079	−2.445 ± 0.071	−3.760 ± 0.058	1.148	33.1	15.7	18.9	14.2
W66	2MIU3984	16470396-4551377	5940106007100719872	1.03	0.101 ± 0.085	−0.078	−2.552 ± 0.108	−3.262 ± 0.090	1.119	17.5	16.0	19.8	14.3
W71	S8UV052000	16470846-4550493	5940106037148742272	0.88	0.065 ± 0.066	−0.069	−2.384 ± 0.084	−4.054 ± 0.081	1.128	97.2	13.2	17.0	11.7
W74	S8UV052684	16470708-4550130	5940199877892578816	0.96	0.061 ± 0.060	−0.077	−2.534 ± 0.075	−4.097 ± 0.070	1.149	68.0	15.2	18.4	13.7
W78	S8UV053443	16470155-4549580	5940106797374731008	0.96	0.148 ± 0.049	−0.071	−1.984 ± 0.060	−3.474 ± 0.052	1.149	123.9	13.9	17.1	12.4
W84	S8UV052342	16465904-4550284	5940106763014989184	1.00	0.177 ± 0.048	−0.073	−2.544 ± 0.056	−3.655 ± 0.052	1.170	97.1	15.3	18.0	13.8
W228b	2MIU39FQ	16465803-4553008	5940106247618875648	1.01	0.264 ± 0.065	−0.060	−2.266 ± 0.084	−3.645 ± 0.063	1.173	7.6	16.1	18.4	14.6
W232	S8UV049673	16470144-4552351	5940105869661755904	1.02	0.224 ± 0.053	−0.072	−2.348 ± 0.067	−3.694 ± 0.053	1.165	108.3	14.8	17.6	13.3
W243	S8UV049907	16470749-4552290	5940105830990286208	1.15	0.012 ± 0.081	−0.022	−1.574 ± 0.108	−4.036 ± 0.086	1.125	102.6	11.5	15.3	10.0
W265	S8UV053674	16470627-4549238	5940199877886921728	0.98	0.293 ± 0.078	−0.008	−2.431 ± 0.096	−3.500 ± 0.087	1.107	80.7	12.4	17.0	10.8
W373	2MIU2A8Q	16465773-4553200	5940106247618872960	1.00	0.171 ± 0.044	−0.070	−2.502 ± 0.056	−3.797 ± 0.047	1.160	126.1	14.2	17.1	12.7
WR I	2MIU38VN	16470088-4551206	5940106655630578560	0.94	0.151 ± 0.086	−0.064	−1.956 ± 0.122	−3.679 ± 0.097	1.122	15.4	16.3	20.3	14.7
WR N	S8UU115458	16465989-4555255	5940105354265570688	1.02	0.090 ± 0.079	−0.083	−1.773 ± 0.103	−3.730 ± 0.081	1.120	33.7	15.3	19.3	13.7
WR T	S8UV055302	16464628-4547582	5940107106612387968	0.95	0.240 ± 0.055	−0.075	−2.528 ± 0.066	−3.772 ± 0.059	1.153	107.9	15.0	18.0	13.5
1005	S8UV050530	–	5940106689983753728	1.05	0.265 ± 0.069	−0.080	−2.355 ± 0.089	−3.679 ± 0.075	1.135	50.3	15.3	19.0	13.7

Notes: The columns are as follows: (1) Name of the source (the coordinates are listed in Clark et al. (2019)); (2) designation of the source in the GSC 2.3 catalogue; (3) designation of the source in the 2MASS PSC catalogue (Skrutskie et al. 2006); (4) Identification of the Gaia EDR3 source; (5) Renormalized Unit Weight Error; (6) Parallax listed from the Gaia EDR3 and its error; (7) Parallax zero-point correction derived from Lindegren et al. (2021b); (8)-(9) Proper motion in RA and Decl axis and their error; (10) ν_{eff}; (11) Minimum photometric error of the G, BP and RP-bands (in σ units); (12)-(14) Magnitude in the G, BP and RP-bands, respectively.

Table A1.

Table A1 – *continued*

Name	GSC designation	2MASS designation	Gaia EDR3 designation	RUWE	π (mas)	π_{ZP} (mas)	μ_α (mas yr^{-1})	μ_δ (mas yr^{-1})	ν_{eff} (μm^{-1})	min(σ_{phot}) (σ)	G (mag)	BP (mag)	RP (mag)
1006	–	16465443-4553300	5940106208947392640	0.98	0.113 ± 0.102	-0.059	-2.353 ± 0.129	-3.734 ± 0.103	1.164	14.3	16.9	19.9	15.4
1010	S8UV050162	–	5940106625576008320	1.39	0.443 ± 0.143	-0.055	-1.991 ± 0.188	-3.844 ± 0.153	1.179	15.7	17.5	19.8	16.0
1016	S8UV049398	16465817-4552470	5940106243307139840	0.97	0.285 ± 0.086	-0.056	-2.103 ± 0.107	-3.639 ± 0.087	1.175	27.7	17.2	19.9	15.7
1019	2MIU398W	16465837-4551488	5940106621270836096	0.98	0.144 ± 0.101	-0.060	-2.305 ± 0.121	-3.770 ± 0.101	1.153	18.8	17.3	20.4	15.8
1020	S8UV049864	–	5940106625576002944	0.97	0.189 ± 0.054	-0.059	-2.552 ± 0.067	-3.410 ± 0.056	1.181	70.9	16.1	18.6	14.7
1021	S8UU115692	16465877-4554319	5940105453031539456	1.01	0.226 ± 0.090	-0.061	-2.160 ± 0.115	-3.290 ± 0.090	1.147	21.6	16.7	20.0	15.1
1028	2MIU398A	16470132-4551385	5940106659927364480	0.97	0.318 ± 0.100	-0.059	-2.102 ± 0.124	-3.298 ± 0.100	1.158	9.5	17.3	20.2	15.7
1029	2MIU38JE	16470150-4549502	5940106793069533568	1.02	0.217 ± 0.092	-0.062	-2.362 ± 0.114	-3.358 ± 0.096	1.144	12.7	16.8	20.1	15.3
1030	S8UV049321	16470167-4552580	5940105869661752192	0.95	0.429 ± 0.047	-0.073	-2.465 ± 0.059	-3.726 ± 0.049	1.159	138.5	14.8	17.8	13.4
1033	S8UV049698	16470235-4552340	5940105869661755648	1.02	0.100 ± 0.069	-0.080	-2.262 ± 0.085	-3.878 ± 0.069	1.148	61.7	15.8	19.1	14.3
1034	S8UV051193	16470254-4551488	5940105904021502976	0.98	0.194 ± 0.061	-0.078	-2.236 ± 0.076	-3.615 ± 0.063	1.156	41.9	15.8	18.8	14.3
1037	S8UV052778	16470285-4550066	5940106797374729344	0.88	0.188 ± 0.068	-0.062	-2.272 ± 0.085	-3.539 ± 0.071	1.144	14.7	16.4	19.7	14.9
1038	S8UV054160	–	5940200629515963136	1.04	0.340 ± 0.181	-0.026	-2.933 ± 0.245	-3.355 ± 0.183	1.303	38.5	18.3	19.5	17.2
1040	S8UV052764	–	5940106797374728576	1.22	0.391 ± 0.089	-0.079	-2.103 ± 0.110	-3.409 ± 0.091	1.149	38.6	15.7	18.7	14.2
1046	S8UV053170	–	5940199873591749632	0.92	0.168 ± 0.065	-0.060	-2.063 ± 0.080	-3.611 ± 0.073	1.157	27.6	16.1	19.0	14.6
1049	S8UV055733	16470667-4547384	5940200771245787008	0.95	0.161 ± 0.056	-0.074	-2.344 ± 0.069	-3.785 ± 0.060	1.128	76.1	14.1	17.9	12.5
1050	S8UV053039	16470677-4549554	5940199877886909696	0.92	0.226 ± 0.074	-0.061	-2.369 ± 0.090	-3.688 ± 0.081	1.150	23.8	16.4	19.6	14.9
1052	S8UV049235	16470699-4552560	5940105835302011776	1.03	0.168 ± 0.135	-0.055	-2.552 ± 0.175	-3.711 ± 0.135	1.147	11.3	17.7	21.0	16.2
1058	S8UV146458	–	5940105972740981120	0.96	0.029 ± 0.098	-0.065	-1.863 ± 0.129	-3.893 ± 0.110	1.123	10.9	16.7	20.7	15.1
1062	–	16471063-4550465	5940199809167415680	0.99	0.189 ± 0.087	-0.061	-2.103 ± 0.107	-3.831 ± 0.088	1.151	16.4	16.9	20.1	15.4
1063	–	16471074-4549476	5940199907951488640	1.00	0.037 ± 0.079	-0.061	-2.220 ± 0.093	-3.777 ± 0.080	1.148	21.8	16.4	19.7	14.8
W19	–	16470485-4550593	5940106007100730368	1.51	-0.052 ± 0.086	–	-2.50 ± 0.11	-3.90 ± 0.09	1.138	67.1	14.4	18.1	12.7
W56a	S8UV050674	16465894-4551486	5940106621264278784	1.59	0.130 ± 0.082	–	-2.38 ± 0.10	-3.44 ± 0.09	1.144	94.9	14.1	17.4	12.5
W238	S8UV049975	–	5940105904021494144	3.62	0.496 ± 0.194	–	-3.26 ± 0.24	-4.90 ± 0.19	1.150	76.9	14.5	17.5	12.9
W28	S8UV052693	–	5940106037148748416	4.50	-0.232 ± 0.168	–	-2.05 ± 0.22	-2.99 ± 0.20	1.149	123.9	13.6	16.8	12.0
W241	S8UV050263	–	5940105899709768192	4.79	0.914 ± 0.25	–	-6.87 ± 0.32	-5.08 ± 0.24	1.150	68.3	15.1	18.2	13.4

Table A2. List of known Westerlund 1 members with Gaia-EDR3 counterparts associated with a 6-parameter astrometric solution (6-p). This table is available online at the CDS.

Name	GSC designation	2MASS designation	Gaia EDR3 designation	RUWE	π (mas)	μ_α (mas yr^{-1})	μ_δ (mas yr^{-1})	Pseudocolour (μm^{-1})	min(σ_{phot}) (σ)	G (mag)	BP (mag)	RP (mag)
W20	S8UV050219	16470309-4552189	5940105904023386752	1.19	0.337 ± 0.124	-3.085 ± 0.148	-4.119 ± 0.119	1.049	30.0	11.3	16.9	9.7
W25	S8UV112186	–	5940106041452309376	0.74	0.061 ± 0.169	-1.911 ± 0.255	-4.050 ± 0.195	1.043	11.2	16.7	19.3	13.9
W49	S8UV112174	–	5940106763006673664	1.02	-0.089 ± 0.475	-3.200 ± 0.615	-2.892 ± 0.436	1.317	111.3	19.4	–	–
W62a	2MIU3988	16470248-4551380	5940106659935750144	0.98	-0.253 ± 0.165	-2.019 ± 0.631	-3.361 ± 0.402	1.115	260.1	16.8	–	–
WR W	2MIU3H42	16470761-4549222	5940199907954832768	1.07	0.062 ± 0.177	-2.077 ± 0.217	-3.614 ± 0.179	1.068	7.0	18.1	21.5	16.5
WR X	–	16471413-4548320	5940199967670849152	1.17		-2.032 ± 0.217	-3.629 ± 0.179	1.137	111.9	–	–	16.3
1002	S8UV049418	16464964-4552530	5940106281978531200	1.12	-0.004 ± 0.135	-2.245 ± 0.164	-3.991 ± 0.134	1.040	58.8	16.3	18.8	14.8
1003	S8UV050318	16465234-4552032	5940106312026629376	0.99	0.314 ± 0.099	-2.395 ± 0.129	-3.688 ± 0.108	1.129	27.7	17.0	19.8	15.6
1007	S8UV052780	–	5940106831734470272	1.02	0.306 ± 0.088	-2.370 ± 0.109	-3.572 ± 0.093	1.126	32.3	16.1	19.7	14.6
1009	S8UV050785	–	5940106694295493376	1.04	0.077 ± 0.087	-2.693 ± 0.106	-3.801 ± 0.092	1.124	23.3	16.2	19.2	14.6
1011	S8UV050317	–	5940106625576009344	1.38	0.533 ± 0.124	-2.856 ± 0.152	-3.811 ± 0.127	1.145	40.3	16.8	19.4	15.3
1012	S8UV137923	–	5940106728646925952	1.09	0.221 ± 0.109	-2.217 ± 0.132	-3.933 ± 0.113	1.109	18.1	17.0	20.7	15.4
1014	S8UV051272	–	5940106659927411456	1.07	0.204 ± 0.094	-2.453 ± 0.114	-3.623 ± 0.099	1.160	33.9	17.0	19.9	15.5
1015	S8UV050784	16465798-4551408	5940106625576014976	0.90	0.201 ± 0.090	-2.192 ± 0.117	-3.740 ± 0.094	1.084	33.5	16.2	19.5	14.7
1017	–	16465824-4550341	5940106827422726784	1.03	0.243 ± 0.102	-2.454 ± 0.124	-3.543 ± 0.107	1.121	7.5	17.0	19.6	15.4
1018	–	16465824-4550570	5940106655624030720	1.00	0.334 ± 0.094	-2.023 ± 0.115	-3.883 ± 0.099	1.113	26.5	16.6	20.0	15.0
1023	–	16470016-4551104	5940106659935760768	1.00	0.286 ± 0.095	-2.243 ± 0.115	-4.298 ± 0.106	1.110	26.7	16.2	19.6	14.6
1024	S8UV051649	16470079-4551019	5940106763014978304	1.10	0.052 ± 0.097	-2.542 ± 0.116	-3.691 ± 0.103	1.122	26.6	16.1	19.5	14.5
1025	–	16470075-4552048	5940106659935744512	1.05	-0.043 ± 0.099	-2.379 ± 0.122	-3.917 ± 0.100	1.170	2.6	17.2	18.4	15.4
1026	2MIU38JC	16470103-4549490	5940106793069532544	1.05	0.181 ± 0.106	-1.967 ± 0.129	-3.360 ± 0.111	1.120	12.9	17.1	20.4	15.6
1027	2MIU38K4	16470103-4550069	5940106797374730240	1.12	0.156 ± 0.115	-2.272 ± 0.140	-3.773 ± 0.120	1.095	9.7	16.9	21.2	15.2
1032	S8UV052545	–	5940106797366425856	1.03	-0.020 ± 0.127	-1.962 ± 0.151	-3.903 ± 0.130	1.112	12.1	17.5	21.0	16.0
1042	S8UV050292	–	5940105904013082240	1.15	0.846 ± 0.358	-10.050 ± 0.886	-12.600 ± 0.488	1.454	276.1	18.7	–	–
1053	–	16470737-4548501	5940199912252322304	1.16	0.088 ± 0.110	-2.282 ± 0.138	-3.720 ± 0.115	1.091	12.0	15.9	20.5	14.3
1056	S8UV051666	16470870-4551016	5940106041460464256	1.93	-0.546 ± 0.267	-2.18 ± 0.36	-1.69 ± 0.31	0.992	17.7	16.5	20.3	14.8
1061	S8UV146498	16470974-4550402	5940199804872244864	0.97	–	-2.307 ± 0.153	-4.283 ± 0.129	1.091	164.4	–	–	16.0
1064	S8UV138096	–	5940199843532840320	1.13	-0.054 ± 0.152	-1.948 ± 0.198	-3.972 ± 0.159	1.050	6.7	17.5	21.8	15.8
1065	S8UV053673	16471160-4549226	5940199912252320128	0.98	0.146 ± 0.095	-2.202 ± 0.116	-4.099 ± 0.101	1.085	44.9	15.3	19.1	13.7
1067	2MIU3H39	16471338-4549106	5940199466612058880	0.95	0.048 ± 0.094	-1.993 ± 0.121	-3.624 ± 0.102	1.095	60.8	15.0	18.9	13.4
1069	S8UU115903	16472417-4553292	5940102742925551616	1.31	0.190 ± 0.139	-2.319 ± 0.186	-3.961 ± 0.149	1.048	6.7	15.5	21.1	13.7

Notes: The columns are as follows: (1) Name of the source (the coordinates are listed in Clark et al. (2019)); (2) designation of the source in the GSC 2.3 catalogue; (3) designation of the source in the 2MASS PSC catalogue (Skrutskie et al. 2006); (4) Identification of the Gaia EDR3 source; (5) Renormalized Unit Weight Error; (6) Parallax listed from the Gaia EDR3 and its error; Lindegren et al. (2021b); (7)-(8) Proper motion in RA and Decl axis and their error; (9) Pseudocolour; (10) Minimum photometric error of the G, BP and RP-bands (in σ units) (11)-(13) Magnitude in the G, BP and RP-bands, respectively.

Table A3. List of known Westerlund 1 members with no astrometric information. This table is available online at the CDS.

Name	GSC designation	2MASS designation	Gaia EDR3 designation	Name	GSC designation	2MASS designation	Gaia EDR3 designation
W1	–	–	–	WR B	–	–	–
W6b	–	–	–	WR C	–	–	–
W8b	–	–	–	WR D	–	–	–
W9	S8UV052695	16470414-4550312	5940106797374722688	WR G	–	–	–
W14c	–	–	–	WR H	–	–	–
W15	–	–	–	WR J	–	–	–
W17	–	–	–	WR K	–	–	–
W18	S8UV052696	16470570-4550506	–	WR O	2MIU39AQ	16470763-4552352	–
W27	S8UV112081	–	5940106041460655744	WR Q	–	–	–
W29	–	–	–	WR U	–	–	–
W30	–	–	–	WR V	–	–	–
W31	–	–	–	1001	S8UV137517	16464919-4553101	5940106178899314432
W34	–	–	–	1004	–	–	–
W36	S8UV111999	16470508-4550553		1008	–	–	–
W37	–	–	–	1013	S8UV049740	–	–
W38	–	–	–	1022	–	–	–
W41	S8UV111985	–	5940106763014977152	1031	–	–	–
W43a	–	–	–	1035	–	–	–
W43b	–	–	–	1036	–	–	–
W43c	S8UV111984	–	5940106007092379904	1039	–	–	–
W44	–	–	–	1041	–	–	–
W46a	–	–	–	1043	–	–	–
W46b	–	–	–	1044	–	–	–
W50b	S8UV052712	–	5940106763006683136	1045	S8UV050529	–	5940106007092303360
W53	–	–	–	1047	S8UV049738	16470612-4552320	–
W56b	–	–	–	1048	2MIU38UI	16470625-4551042	–
W57c	–	–	–	1051	2MIU3H55	16470701-4549405	–
W61a	S8UV051190	16470231-4551416	–	1054	–	–	–
W61b	–	–	–	1055	–	–	–
W70	S8UV052001	16470938-4550496	–	1057	–	–	–
W72	–	–	–	1059	S8UV048805	16470907-4553204	–
W75	2MIU38JS	16470892-4549585	–	1060	–	–	–
W86	–	–	–	1066	–	–	–
W237	S8UV050219	16470309-4552189	–	1068	S8UV050802	–	5940199603008974464
W239	–	–	–				

Notes: The columns are as follows: (1) Name of the source; (2) designation of the source in the GSC 2.3 catalogue; (3) designation of the source in the 2MASS PSC catalogue (Skrutskie et al. 2006); (4) Identification of the source in the Gaia EDR3 catalogue (no astrometry is available).

This paper has been typeset from a TEX/LATEX file prepared by the author.